ISSN 0016-7029, Geochemistry International, 2016, Vol. 54, No. 2, pp. 149–166. © Pleiades Publishing, Ltd., 2016.
Original Russian Text © V.L. Tauson, D.N. Babkin, T.M. Pastushkova, N.V. Smagunov, S.V. Lipko, I.Yu. Voronova, V.I. Men'shikov, N.V. Bryanskii, K.Yu. Arsent'ev, 2016, published in Geokhimiya, 2016, No. 2, pp. 165–181.

Dualistic Distribution Coefficients of Trace Elements in the System Mineral–Hydrothermal Solution. III. Precious Metals (Au and Pd) in Magnetite and Manganmagnetite

V. L. Tauson[a], D. N. Babkin[a], T. M. Pastushkova[a], N. V. Smagunov[a], S. V. Lipko[a], I. Yu. Voronova[a], V. I. Men'shikov[a], N. V. Bryanskii[a], and K. Yu. Arsent'ev[b]

[a] *Vinogradov Institute of Geochemistry, Siberian Branch, Russian Academy of Sciences, ul. Favorskogo 1a, Irkutsk, 664033 Russia*

[b] *Institute of Limnology, Siberian Branch, Russian Academy of Sciences, ul. Ulan-Batorskaya 3, Irkutsk, 664033 Russia*

e-mail: vltauson@igc.irk.ru

e-mail: arskir@gmail.com

Received April 21, 2014; in final form, August 25, 2014

Abstract—Distribution coefficients D of Au and Pd between magnetite (manganmagnetite) and ammonium chloride hydrothermal solution and the structural D^{str} and surface-related D^{sur} terms of these coefficients were determined at 450 and 500°C and a pressure of 1 kbar using internal sampling techniques. Quantitative data on the speciation of precious metals are obtained using the technique of statistical selections of analytical data on single crystals SSADSC and compared with LA-ICP-MS data. Both Pd and Au are elements compatible with magnetite and its manganoan variety: D^{str} is ≈3 for Pd and ≈1 for Au, although Au seems to weakly enrich fluid at 500°C: $D^{str} \approx 0.5–0.8$. The trends of postmagmatic Pd and Au fractionation can thus strongly depend on the presence of spinel-group minerals, first of all, magnetite and its solid solutions. The dualistic nature of the distribution coefficients provides sound grounds to believe that both elements are highly compatible, with regard not only for the structural but also for the surface-related modes of their occurrence ($D^{sur} \approx 17$ and ≈50–70 for Au and Pd, respectively). The maximum concentrations of structural modes of the elements are 5.3 ppm for Au and 5.1 ppm for Pd and were found in the solid solution whose jacobsite mole fractions were 0.82 and 0.49, respectively. The principal distribution patterns of the elements in crystals are confirmed by LA-ICP-MS data. Data on this system testify that the distribution coefficients of minor and trace elements are geochemically dualistic because of the abnormal absorption properties of nanometer-sized nonautonomous phases on the surface of ore minerals, and this dualism plays an important geochemical role.

Keywords: distribution coefficient, hydrothermal solution, gold, palladium, magnetite, manganmagnetite, structural mode of occurrence, surface-related mode of occurrence, nonautonomous phase

DOI: 10.1134/S0016702916020063

INTRODUCTION

This publication continues a series of our earlier papers devoted to the dualistic nature of the distribution coefficients of minor elements in fluid–mineral systems (Tauson et al., 2011, 2012). Our earlier results, which were lately appended with newly obtained natural data (Tauson et al., 2014), can be summarized as follows. Very thin (no thicker than a few hundred nanometers) layers of surface phases may occur on the surface of crystals of ore minerals. These phases are able to uptake much minor and trace elements, first and foremost, so-called incompatible ones, which are merely insignificantly accommodated in the structures of the minerals. Of course, information on the equilibrium fluid phase derived from this mode of occurrence of an element is principally different from information obtained from the structural admixture of this element contained in the volume of the mineral crystal (i.e., in its structure). The distribution coefficient of the minor element is thus of dualistic nature, with the "surface" coefficient significantly exceeding the "structural" one. Inasmuch as only the latter can adequately reflect the concentration of the element in the solution (according to Henry's law), it is necessary to distinguish between two constituents of an admixture of an element: one structural (volumetric) and the other related to nanometer-sized phases on the surface of mineral crystals (surface-related component of the admixture). To do this, we have developed specialized techniques: analysis of statistical selections of analytical data on single crystals, SSADSC. Pyrite from gold deposits (regardless of their genetic types, age, and parameters of their mineral-forming processes) has

been proved to contain Au in two major modes: equally distributed in grain volumes (structural mode) and surface-related (surface mode), with the latter commonly being dominant. In the overwhelming majority of instances, gold equally distributed in pyrite is a mode in which gold occurs in a state chemically bound to the structure of the mineral and the structures of nanometer-sized nonautonomous phases on the surface of pyrite crystals. The dependence of the concentration of equally distributed gold on the grain size of its host pyrite and the restriction of much of this gold to the crystal surfaces seems to be a common characteristic of ore minerals of hydrothermal genesis (Tauson et al., 2014).

Very little information on the origin of so-called transient minerals (i.e., those that can be formed within broad ranges of physicochemical parameters and thus can be formed by diverse geochemical processes and in various environments) can be derived from the equilibrium relations of these minerals with others and from their bulk chemical compositions. One of such minerals is magnetite: it can occur both in cumulus associations and in rocks and ores modified by younger hydrothermal processes, as for example, at magmatic Cu–Ni deposits with PGE. Minor-element composition of magnetite usually adequately reflects its genetic traits. For example, at copper porphyry deposits with PGE and Au, Cr-bearing magnetite is typical of the mantle or deep crustal source, whereas Cr-free magnetite is found in younger quartz veins (Economou-Eliopoulos and Elipoulos, 2005). At the same time, Cr-spinel in the well known Merensky Reef is interpreted by some researchers as a cumulus phase and is believed to be a late crystallization product by others (Crocket et al., 1976). It is pertinent to mention that the possibility of the preservation of primary magmatic distributions of elements during younger postmagmatic, tectonic, hydrothermal, and metamorphic processes is disputable (Collins et al., 2012). For example, magnetite can be formed through pyrrhotite oxidation, but it is hard to say how much can it thereby inherit PGE composition from the primary magmatic sulfides in the absence of data on the distribution coefficients of these elements between magnetite and fluid. Another conceivable mechanism able to form magnetite is the crystallization of Fe-rich monosulfide solid solution (Naldrett et al., 2000). Correlations between the proportions of PGE and trace elements in the magnetite testify that variations in these proportions in magnetite could be controlled by the fractionation of sulfide liquid (Dare et al., 2011). Furthermore, younger hydrothermal solutions could introduce other elements, and the PGE proportions in that magnetite can significantly differ from that of the original sulfide ore. Such relations were extensively described in the literature and pertain not only to magnetite. For example, PGE-bearing pyrite at the Aguablanca Ni–Cu deposit in Spain inherits certain PGE (Os, Ir, Ru, and Rh) from the replaced pyrrhotite and was enriched by other elements (Pd, Au, and others) brought by younger hydrothermal fluids of magmatic provenance (Piña et al., 2013).

Much importance is attached to the modes of PGE occurrence and their distribution coefficients when models are developed to describe concentration of these elements at ore deposits. Numerical models make use of mineral–fluid and mineral–melt distribution coefficients. While several mineral–melt distribution coefficients were determined experimentally, such data on mineral–fluid distribution coefficients are usually absent, and these are assumed based on various considerations and speculations (Boudreau and Meurer, 1999). At the same time, there are data suggesting that Pt and Pd chloride complexes could occur in magmatic fluids during the early crystallization of chromite (Vatin-Perignon et al., 2000). The deposition of precious metals from high-temperature fluid phases is understood still relatively poorly, but it is hypothesized that Cl-bearing fluids could appear very early in the course of the differentiation process. The partial remobilization of precious metals (Pt, Pd, and Au) by low-temperature fluids is of secondary nature. The applicability of experimental data on the solubility of various phases in studying naturally occurring ore-forming systems is, in fact, largely defined by the phase that controls the concentrations of the element in the solution (Xioing and Wood, 2000; and others). Our earlier results demonstrate that minor and trace elements (Au and PGE) can be buffered not only (and even not so much) by their individual phases but also (and often mostly) by surface nonautonomous phases that contain relatively much these elements (Tauson et al., 2013). Moreover, the concentrations of a structural admixture of a minor or trace element can be utilized to estimate the concentration of this element in the ore-forming fluid, as was demonstrated for Au in (Tauson et al., 2014). Gold, platinum, and palladium are the most widely spread precious metals (Chyi and Crocket, 1976), and such estimates can be made for them, but only if the distribution coefficients for their structural modes are known. Recent progress in analytical techniques of high spatial resolution makes it possible to readily obtain data on the composition of fluids by analyzing inclusions in mineral crystals. However, experimental data indicate that principal constraints are imposed by diffusion-driven reequilibration and postgrowth changes in the concentrations of elements in inclusions, with these changes amounting to one to three orders of magnitude for certain ore elements (Zajacz et al., 2009). This calls for very accurate experimental tests in each particular instance.

Not constraining our considerations to the purely geochemical aspects of the problem, it is pertinent to note that precious metals traditionally attract keen interest as catalysts of various chemical processes. Ferrites of transition metals (such as magnetite and its solid solutions) activated with palladium and other

Table 1. Experimental parameters and analyses of fluid in experiments on the synthesis of crystals in the systems Fe–O– and Fe–Mn–O–hydrothermal solution at a pressure of 1 kbar

Experimental run, T, °C	Starting materials				Composition (wt %) of starting solution	In traps after experiments				
		wt %				wt %		ppm		pH
	$\frac{Me^{ox}}{FeO}$ (mol)*	Fe_2O_3	FeO	Mn_2O_3		Fe	Mn	Au	Pd	
D12-4, 450	0.2	–	69.5	30.5	10% NH_4Cl	0.84	2.26	0.22	2.2	8.8
D13-2, 450	1	62.14	31.03	6.83	8% NH_4Cl + 2%HCl	2.72	0.18	0.49	0.45	8.4
D13-3, 450	1	55.27	31.07	13.66	The same	1.86	0.93	0.52	0.93	8.3
D17-3, 450	0.5	–	47.6	52.4	⋘	0.11	2.32	0.46	1.27	8.5
D18-3, 450	1	69	31	–	10% NH_4Cl	1.55	0.03	1.13	0.78	8.5
D18-4, 450	1	69	31	–	8% NH_4Cl + 2% HCl	1.69	0.01	0.15	0.22	8.5
D18-6, 450	0.5	–	47.62	52.38	The same	0.41	4.32	2.36	1.45	8.0
D19-4, 500	0.5	–	47.62	52.38	⋘	0.30	4.68	0.23	0.30	8.0
D19-5, 500	0.5	–	47.62	52.38	10% NH_4Cl	1.51	23.59	0.25	0.30	8.4
D20-1, 500	1	69	31	–	The same	8.65	0.07	0.29	0.79	8.8
D20-3, 500	1	69	31	–	⋘	7.17	0.04	0.23	0.21	8.8
D21-5, 500	0.5	–	47.62	52.38	⋘	0.40	6.40	2.21	1.57	9.0
D22-1, 500	0.3	–	60.24	39.76	⋘	6.80	31.7	1.60	0.49	8.5

* Mole ratios of oxidized modes ($Fe_2O_3$and Mn_2O_3) to FeO; in experimental runs D12-4, D13-2, D13-3, D17-3, and D20-3, the amount of oxides in the starting materials was 3 g, and those in other runs was 5 g.

precious metals are promising as oxidation catalysts of carbon monoxide (Radhakrishnan Nair and Aniz, 2013). The speciation of elements and the size of their naturally occurring species and their chemical nature on the surface of other phases undoubtedly play an important role in their catalytic activity (Belykh et al., 2013).

The considerations presented above predetermined our choice of magnetite and its solid solutions with $MnFe_2O_4$ as a mineral matrix and precious metals (Au and Pd) as minor elements in studying the dualistic nature of the distribution coefficient.

EXPERIMENTAL AND ANALYTICAL TECHNIQUES

As in our earlier studies within the framework of this project, we utilized thermogradient hydrothermal synthesis with internal sampling. The experiments were carried out in stainless steel autoclaves approximately ~200 cm^3 in volume with inserts of VT-8 titanium-based alloy. The inserts were equipped with traps made of the same material. The temperature in the zone of crystal growth was 450 or 500°C, the temperature gradient along the autoclave wall was 15°C, and the pressure was 100 MPa (1 kbar). The compositions of the starting solid materials and solutions are reported in Table 1. The reactants were of the following classes of purity: reagent-grade for Fe_2O_3, especially pure for Mn_2O_3, pure for FeO, and especially pure for NH_4Cl; Au and Pd were introduced into the starting materials in the form of foil (99.99%) and coiled wire (99.9%), respectively, in amounts of 1% of the total amount of the material (3 or 5 g).

As in our previous studies (Tauson et al., 2011, 2012), the experiments were conducted in two stages: isothermal and gradient. Their durations were 3 and 15 days, respectively, at a temperature of 500°C and 4 and 20 days, respectively, at 450°C. The experiments were terminated with quenching the autoclaves with cold water. Analyses of the fluid captured in the traps for major (Fe and Mn) and minor (Au and Pd) elements and the pH of the solution are presented in Table 1. The analytical procedures are described in detail in (Tauson et al., 2012). To completely extract the elements from the traps, the latter were washed with *aqua regia*.

The analytical information was obtained mostly by atomic absorption spectrometry (AAS). Iron and manganese in fluid and manganese in magnetite were analyzed by AAS on an AAnalyst-200 (Perkin-Elmer) spectrophotometer accurate to ±2%. In analyzing magnetite crystals for precious metals, we applied electrothermal atomic absorption spectrometry (ETAAS) in its SSADSC version (Tauson et al., 2011, 2012, 2014). While Au can be reasonably accurately analyzed directly in solution (after the decomposition

of the crystal) accurate to ±12% (detection limit 0.3 ppb), Pd was determined in an aliquot of the same solution after its preparatory extraction concentrating and separation from the matrix (Men'shikov et al., 2009). The extractant was tristyrylphosphine $(C_6H_5CH{-}CH)_3P$. Extraction was carried out in weak (0.5 M) HCl solutions. The concentration of the extractant was 0.05 M (in toluene), and the phase were in contact for 30 min (for Pd). The volumetric proportion of the aqueous and organic phases was 2 : 1. Extraction was conducted in static mode, at room temperature, without any labilizing agents. Concentrations of chemical elements were analyzed in the organic phase. The concentrations were measured by ETAAS on a Perkin-Elmer (models 503 and AAnalyst-200) accurate to ±10% (detection limit 5 ppb).

In its most accurate version, our original SSADSC techniques used to distinguish between modes of precious-metal occurrence (Tauson et al., 2011, 2012; 2013; 2014) requires that a large enough numbers of single crystals were obtained in each experiment and that these crystals have clean surface and good natural faceting and vary in size, which is sometimes hard to achieve. These conditions are usually met by less than 30% of the experiments. The SSADSC data-processing routine is described in much detail in the aforementioned papers. The whole massif of analytical data on crystals is subdivided into mass ranges in such a way that all ranges comprises roughly equal numbers of crystals (if possible, no less than 15 crystals per range), with as little as possible spread in the crystal masses in each selection and with regard for the "quality" of the internal statistics of each selection and the representativeness of discrete size fractions. Average concentrations and root mean-square deviations s were then determined for each range. Values >1s were rejected as not meeting the criterion of equal distribution. Negative deviations (more than 1s) were left in the selections because a crystal can contain (in principle) any low concentration of a structural admixture. After this a new average and its standard error ±σ was calculated.

Finally a procedure for distinguishing between structural and surface-related modes was applied. To do this, we used a criterion according to which a concentration value of a precious metal C_{PM} within any given range of crystal sizes (masses) should be rejected if this value is greater than $\overline{C}_{PM}$ + 30% $\overline{C}_{PM}$, defining the possible variations in the structural mode concentration (Tauson et al., 2011; 2012, 2014). Then an average concentration of the equally distribution mode of precious metals $\overline{C}_{PM} \pm \Delta$ was found for each size fraction, and the corresponding average crystal mass $\overline{m}$ and specific surface area $\overline{S}_{spe} = K\overline{r}^2/\overline{m}$ were calculated for each range crystal sizes. The shape of the crystals was approximated with an octahedron whose edge is $\overline{r}$ in length (K is the shape factor). At a large enough number of the size fractions (⩾4), the concentration of the structural admixture of precious metals was determined by constructing dependences for the selections in the form $\overline{C}_{PM} = ke^{n\overline{S}_{spe}}$. The extrapolation of $\overline{C}_{PM}$ to $\overline{S}_{spe}$ leads to $\overline{C}_{PM} = k$, which characterizes a virtual crystal possessing a zero specific surface. As is demonstrated in our earlier publications (Tauson and Lustenberg, 2008; Tauson et al., 2013), this corresponds to the concentrations of the structural mode of a minor element C^{str} accurate to ±30%.

For the contributions of various modes of occurrence of precious metals to be comparable with one another, we introduce the concept of a surface-related mode (Tauson et al., 2014). The concentration corresponding to this mode characterizes an average crystal in each size fraction, i.e., the corresponding surface-related excess concentration of the element

$$\overline{C}^{sur} = \frac{\Sigma(\overline{C}^s - C^{str})n^s\overline{m}^s}{\Sigma n^s\overline{m}^s}, \quad (1)$$

where $\overline{C}^s$ is the average concentration of the equally distributed mode of the precious metals in each size fraction s with a number of crystals n^s and an average crystal mass $\overline{m}^s$.

The surface distribution coefficient D^{sur} is normalized to this value, but not to the mass of the nonautonomous phase (NP), as was done previously (Tauson et al., 2011, 2012), which is more convenient because it is now not necessary to make any assumptions about the characteristics of the surface NP: the thickness of its layer, the extent to which this layer covers the surface, etc. This allows us to compare the contributions of the surface and volume modes to the bulk content of the element, although it must be borne in mind that the concentrations of distinct modes are not additive values, and additive ones are the corresponding quantities of substance.

A few samples were analyzed by LA-ICP-MS on a Perkin-Elmer NexION 300D quadrupole mass spectrometer equipped with a NWR-213 laser ablation system at the Vinogradov Institute of Geochemistry, Siberian Branch, Russian Academy of Sciences, in Irkutsk. The technique is described in detail below.

The phase composition of the products was analyzed and the unit-cell parameters were determined on a D8 ADVANCE (BRUCKER) diffractometer accurate to $a_o \pm 1 \times 10^{-5}$ nm.

EXPERIMENTAL RESULTS AND THEIR INTERPRETATION

Synthetic phases. The crystals of "pure" magnetite synthesized at 450°C reached 2 mm across and were dominated by variably flattened octahedra and more rare twins and cuboctahedra. The surfaces of the crystals that were in contact with fluid are often covered with brown fine-grained hematite (quench phase). If

$Mn_2O_3$was added to the starting materials, the crystals in the experimental products were much smaller (~1 mm), and their shapes were more complicated: the experimental products contained more cuboctahedra complicated with {110} faces. Still most crystals in all instances ("pure" magnetite and Mn-magnetite) had the shapes of flattened octahedra. At 500°C, the largest crystals of "pure" magnetite were larger (up to 2.5 mm), whereas the Mn-magnetite crystals were no larger than 1.5 mm. The dominant simple crystal forms were {111} or {111 + 100}. The precious metals added to the system were preserved in the materials of all successful experimental runs but were corroded (this pertains, first of all, to the Pd wire, which was sometimes disintegrated); whereas Au foil became brittle but was corroded not so significantly. The occurrence of fine-grained hematite as a quench phase in runs with low Mn concentrations and the appearance of relatively large hematite crystals in the growth zone when even little (6 wt %) Cr_2O_3 was added to the system suggest that the experimental parameters were close to the magnetite–hematite equilibrium line: $\log fO_2 \leq -21.6$ at 450°C and ≤ -19.2 bar at 500°C.

Figure 1 shows the dependence of the unit-cell parameter of the magnetite–jacobsite solid solution on the $MnFe_2O_4$ molar concentration. In the general case, this dependence is of complicate nonlinear character because the parameter a_0 is a function not only of the Mn concentration but also of its valence and the degree major of the structure inversion (Taroev and Tauson, 1984).

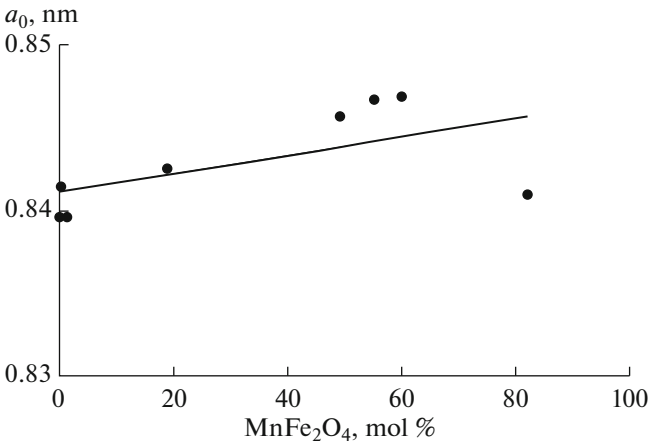

Fig. 1. Unit-cell parameter of synthesized magnetite as a function of concentration of the jacobsite end member.

Distribution of major components. Tables 1 and 2 present data on the concentrations of major components (Fe and Mn) in the fluid captured in the traps and in the synthetic magnetite crystals. The cocrystallization coefficient, which was calculated as $D_{Mn/Fe} = (Mn/Fe)_{mt}/(Mn/Fe)_{aq}$ for NH_4Cl and NH_4Cl + HCl solutions was 0.009 ± 0.002 at 450°C and 0.014 ± 0.002 at 500°C. The coefficient does not vary within a broad range of the Mn/Fe ratio of about three orders of magnitude. However, at very low Mn concentrations in the solution (a few hundredths of a percent), $D_{Mn/Fe}$ increases to 0.04 ± 0.01. A similar increase in the distribution coefficient was previously detected at low Mn concentrations in sphalerite and galena and was explained by the accommodation of minor admixtures at structural defects, including those on the surface of the crystals (Akimov and Tauson, 2003). It will be demonstrated below that the reason for the increase in D in our situation is an Mn enrichment in the surface magnetite layer. Clearly defined dependences obtained at higher concentrations (Table 2) justify the

Table 2. Mn and Fe cocrystallization coefficients in magnetite from NH_4Cl and (NH_4Cl + HCl) hydrothermal solutions at 450 and 500°C

Experimental run	T, °C	mol % $MnFe_2O_4$ in Mt	$(Mn/Fe)^{Mt}_{at}$	$(Mn/Fe)^{aq}_{at}$	$D^*_{Mn/Fe}$	$\bar{D}_{Mn/Fe} \pm \Delta$
D17-3**	450	37.4	0.14	21.4	0.007	0.009 ±0.002
D13-2**	450	0.2	0.00067	0.067	0.01	
D13-3**	450	1.3	0.0044	0.508	0.009	
D12-4	450	8.8	0.03	2.73	0.011	
D19-4**	500	60.1	0.25	15.86	0.016	0.014 ± 0.002
D19-5	500	55.3	0.226	15.86	0.014	
D21-5	500	49.2	0.196	16.27	0.012	
D22-1	500	18.8	0.067	4.74	0.014	
D18-4**	450	0.08	0.00027	0.006	0.046	0.04 ± 0.01
D20-1	500	0.08	0.00027	0.0077	0.035	
D20-3	500	0.08	0.00027	0.0054	0.05	

* $D_{Mn/Fe} = (Mn/Fe)^{Mt}/(Mn/Fe)^{aq}$. ** Starting solutions were 8% NH_4Cl + 2% HCl and 10% NH_4Cl in other instances; no Mn was introduced into the system in the three last experimental runs.

selection of the fluid sampling technique for this study.

SSADSC data. Analyses of individual magnetite crystals synthesized in the experiments are presented in Tables 3 and 4 for Au and Pd, respectively. Data in these tables specify the mass and size (octahedron edges) ranges, the specific surface area of the average crystals in these ranges, and the average concentrations of evenly distributed precious metals. Figure 2 makes it possible to compare data on the "pure" magnetite (experimental run D20-3, 0.08 wt % $MnFe_2O_4$) and Mn-bearing one (runs D22-1, 18.8 mol % and D21-5, 49.2 mol %) synthesized at 500°C. Such dependences were constructed for all runs whose data are given in Tables 3 and 4 and testify that the surface-related modes of occurrence of the precious metals remarkably affect the distributions of the metals. Regardless of temperature and other parameters of synthesis, these dependences are characterized by high coefficients of determination (0.839–0.999). The preexponential factors in the formulas in Fig. 3 are identified with the concentrations of the structural (volumetric) components of the PM concentrations. The contribution of the surface-related mode defines the slope of the exponential function: the greater this slope, the higher the contribution. Following this interpretation, one can readily realize that the concentrations of the structural PM modes significantly and systematically increase with increasing concentration of the Mn end member of magnetite within the range of 0 to 49 mol % jacobsite (Fig. 2). The concentration of structural Au increases from 0.1 ppm in "pure" magnetite to 3 ppm in Mn-bearing one. Simultaneously, the concentration of structural Pd increases from 0.8 to 5.1 ppm. At the same time, the increase in the Mn concentration is associated with a decrease in the slope of the exponential dependences, which suggests a decrease in the contribution of the surface-related PM modes. This, in turn, provides support for our earlier conclusion, which was based on direct analysis of crystal surfaces (Tauson et al., 2012), that Mn-rich magnetite possesses less nonautonomous phase that is responsible for the adsorption of minor and trace elements by the surfaces of magnetite crystals. At higher concentrations of the Mn end member of magnetite (55.3–60.1 mol %), the concentrations of both the structural and the surface-related modes of Au and Pd occurrence decrease to values typical of "pure" magnetite (Tables 5, 7) and likely increase again (at least for Au) in the Mn richest magnetite whose composition approaches jacobsite (82.2 mol %).

Distribution coefficients of the precious metals. Table 5 reports concentrations of various PM modes and the corresponding dualistic distribution coefficients. Data on Au at 450°C can be compared with those in (Tauson, 2012), which were obtained at the same parameters but in the absence of Pd. The distribution coefficient of structural Au is close to unity and confirms the conclusion that this element is compatible with magnetite, and also with Mn-bearing magnetite. At 500°C, D_{Au}^{str} is slightly lower (0.5), suggesting that Au is weakly preferably redistributed into the fluid phase, but the coefficient of Mn-bearing magnetite is again close to one (0.8 ± 0.5). The distribution coefficient of structural Pd is close to three in both "pure" and Mn-bearing magnetite and at both temperature values. The distribution coefficients of surface-related PM modes are more than one order of magnitude higher than the distribution coefficients of their structural modes (Table 6). In spite of the remarkably broad variations in the concentrations of both structural and surface-related PM modes, their ratios vary incredibly little (Table 6). This demonstrates that the behavior of the nonautonomous phase (NP) is governed by the principle of equilibrium phase correspondence (Tauson, 2009), because of which the occurrence of an element in the structure of a crystal means that this element must also necessarily be contained in the surface nonautonomous phase. The NP containing crystal occurs in metastable "forced" equilibrium (Tauson and Akimov, 1997) with an analogous crystal (or its part) devoid of NP, but their constants of the exchange reactions of an element with the fluid phase are different, and this predetermines a dualistic character of distribution in this situation. In Table 7, the concentrations of the surface-related and structural modes of Au and Pd occurrence are presented as depending on the composition of the solid solution. These dependences are of complicated nature and have maxima (Figs. 3a, 3b).

A certain decrease in the structural D value within the composition range of 49–60 mol % $MnFe_2O_4$ was detected for both Au and Pd (Figs. 3c, 3d). The variations in C^{sur} and C^{str} in this region are much broader, although experimental runs D21-5 and D-19-5 were conducted under closely similar conditions (Table 1). The possible reason of the instability of the system in the compositional region near 50 mol % of the jacobsite end member is fluctuations in temperature and oxygen fugacity toward the field of hematite, a phase that can accommodate much less Mn. These fluctuation may significantly affect the state of elements of variable valence, which are sensitive to the redox potential of the system. This also follows from the composition of fluid in the traps: the Fe and Mn concentrations in run D19-5 are notably higher and the PM concentrations are lower than in run D21-5 (Table 1). The conceivable reason for these differences may also be the not exact identity of the inner surfaces of the Ti inserts, which depends on their previous exploitation histories. In practice, it is not possible to utilize exactly similarly manufactured and preutilized inserts. We have faced this problem when studying the behavior of Hg, another element of variable valence. The problem was then solved by using quartz ampoules

Table 3. Gold concentrations in magnetite and manganmagnetite crystals of various size

Experimental run, T°C	Phase composition*	Mass range, mg	n**	$\bar{m}$, mg	$\bar{r}$, mm	$\bar{S}_{spe}$, mm^2/mg	$\bar{C}_{Au} \pm \Delta$, ppm
D13-2, 450	Mt, 0.2	0.10–0.13	7	0.11	0.354	3.946	10.9 ± 2.1
		0.15–0.26	6	0.23	0.454	3.104	8.6 ± 6.4
		0.27–0.59	4	0.47	0.576	2.445	3.3 ± 2.2
		0.65–1.66	5	1.16	0.779	1.812	1.7 ± 1.1
D13-3, 450	Mt-Mn, 1.3	0.10–0.11	7	0.10	0.343	4.075	8.0 ± 0.9
		0.12–0.13	7	0.13	0.376	3.767	6.3 ± 1.0
		0.14–0.22	8	0.18	0.420	3.395	5.0 ± 0.9
		0.25–0.52	7	0.34	0.517	2.723	3.1 ± 0.5
D18-3, 450	Mt, 0.1	0.09–0.13	9	0.12	0.365	3.846	96.0 ± 30.3
		0.14–0.16	7	0.15	0.395	3.603	76.6 ± 5.6
		0.17–0.23	8	0.19	0.428	3.340	57.4 ± 19.3
		0.27–0.71	9	0.38	0.537	2.629	24.9 ± 7.1
D18-6, 450	Mt-Mn, 82.2	0.19–0.26	5	0.24	0.460	3.054	45.1 ± 19.2
		0.31–0.43	5	0.37	0.532	2.650	34.0 ± 18.4
		0.44–0.55	8	0.49	0.584	2.411	39.6 ± 8.6
		0.57–1.03	8	0.76	0.677	2.089	20.4 ± 2.3
D19-4, 500	Mt-Mn, 60.1	0.16–0.36	6	0.30	0.497	2.852	48.8 ± 23.5
		0.43–0.77	8	0.59	0.621	2.264	12.7 ± 4.3
		0.80–1.17	6	0.97	0.735	1.929	5.0 ± 1.9
		1.24–3.78	6	2.36	0.988	1.433	3.0 ± 1.2
D19-5, 500	Mt-Mn, 55.3	0.26–0.58	6	0.43	0.560	2.526	13.0 ± 7.1
		0.68–0.95	6	0.84	0.700	2.021	8.3 ± 3.1
		1.28–2.30	6	1.88	0.916	1.546	2.2 ± 0.6
		2.45–5.66	6	3.43	1.119	1.265	2.0 ± 0.9
D20-1, 500	Mt	0.11–0.28	6	0.22	0.447	3.146	10.1 ± 3.7
		0.30–0.40	6	0.34	0.517	2.723	3.9 ± 0.9
		0.42–0.58	6	0.48	0.580	2.428	3.1 ± 2.1
		0.60–0.78	8	0.73	0.667	2.111	1.8 ± 0.5
		0.82–1.49	6	1.07	0.759	1.865	2.4 ± 1.0
D20-3, 500	Mt	0.24–0.51	9	0.46	0.572	2.464	6.7 ± 1.2
		0.55–0.73	10	0.67	0.649	2.178	5.2 ± 1.1
		0.75–0.95	9	0.84	0.700	2.021	3.3 ± 1.0
		0.99–1.36	10	1.16	0.779	1.812	4.1 ± 1.1
		1.38–1.94	9	1.64	0.874	1.613	1.6 ± 0.4
		2.01–5.83	8	3.07	1.078	1.311	0.8 ± 0.3
D21-5, 500	Mt-Mn, 49.2	0.09–0.13	5	0.11	0.354	3.946	55.3 ± 19.5
		0.14–0.17	6	0.15	0.395	3.603	40.3 ± 0.2
		0.18–0.21	5	0.20	0.432	3.233	36.2 ± 11.2
		0.23–1.25	6	0.67	0.649	2.178	14.6 ± 12.3
D22-1, 500	Mt-Mn, 18.8	0.09–0.23	8	0.22	0.447	3.146	45.9 ± 12.4
		0.24–0.30	7	0.27	0.480	2.956	26.1 ± 9.6
		0.31–0.37	7	0.34	0.517	2.723	20.6 ± 4.3
		0.38–0.44	10	0.41	0.551	2.565	26.4 ± 5.8
		0.45–0.63	9	0.57	0.616	2.306	11.7 ± 2.2
		0.66–1.85	9	0.93	0.724	1.952	8.8 ± 2.1

* Mt—magnetite, Mt-Mn—Mn-bearing magnetite, mol % of the $MnFe_2O_4$ end member. ** Number of crystals in the final selection.

Table 4. Palladium concentrations in magnetite and manganmagnetite crystals of various size

Experimental run, T°C	Phase, composition *	Mass range, mg	n**	$\bar{m}$, mg	$\bar{r}$, mm	$\bar{S}_{spe}$, mm^2/mg	$\bar{C}_{Pd} \pm \Delta$, ppm
D13-2, 450	Mt, 0.2	0.11–0.22	4	0.18	0.420	3.395	149.7 ± 77.2
		0.26–0.57	3	0.43	0.560	2.256	31.8 ± 7.2
		0.59–0.93	5	0.78	0.683	2.072	24.1 ± 7.3
		0.99–1.81	5	1.46	0.842	1.682	12.3 ± 6.3
D13-3, 450	Mt-Mn, 1.3	0.10–0.12	8	0.11	0.354	3.946	176.3 ± 44.0
		0.13–0.16	7	0.14	0.385	3.668	104.0 ± 43.0
		0.17–0.28	7	0.22	0.447	3.146	79.1 ± 32.9
		0.32–0.98	5	0.67	0.649	2.178	25.6 ± 10.7
D19-4, 500	Mt-Mn, 60.1	0.16–0.36	7	0.29	0.492	2.891	74.7 ± 15.4
		0.43–0.59	7	0.49	0.584	2.411	37.1 ± 4.9
		0.74–1.17	8	0.95	0.729	1.938	18.9 ± 3.3
		1.24–3.78	6	3.14	1.086	1.301	5.5 ± 1.2
D19-5, 500	Mt-Mn, 55.3	0.26–0.50	7	0.42	0.556	2.550	65.1 ± 12.0
		0.58–0.86	7	0.78	0.683	2.072	29.8 ± 5.2
		0.94–1.89	6	1.49	0.848	1.672	17.5 ± 4.3
		1.93–4.41	5	3.78	1.155	1.223	5.7 ± 1.5
D20-1, 500	Mt	0.11–0.28	7	0.22	0.447	3.146	185.3 ± 25.1
		0.30–0.40	7	0.35	0.522	2.697	109.2 ± 25.0
		0.42–0.58	9	0.50	0.588	2.395	79.7 ± 9.3
		0.60–0.78	9	0.73	0.667	2.111	50.5 ± 53.5
		0.82–1.49	6	1.10	0.766	1.848	28.8 ± 5.1
D20-3, 500	Mt	0.24–0.51	11	0.44	0.565	2.513	65.1 ± 8.7
		0.55–0.73	11	0.67	0.649	2.178	37.7 ± 5.1
		0.75–0.95	10	0.86	0.705	2.002	28.2 ± 3.6
		0.99–1.36	11	1.17	0.782	1.811	20.3 ± 1.8
		1.38–1.94	10	1.69	0.883	1.598	13.9 ± 1.4
		2.01–5.83	11	2.93	1.061	1.331	7.8 ± 1.2
D21-5, 500	Mt-Mn, 49.2	0.09–0.13	6	0.11	0.354	3.946	192.5 ± 49.0
		0.14–0.17	4	0.17	0.412	3.459	115.1 ± 33.7
		0.18–0.21	8	0.20	0.432	3.233	125.0 ± 21.4
		0.23–1.25	6	0.54	0.604	2.340	42.5 ± 22.9
D22-1, 500	Mt-Mn, 18.8	0.09–0.24	7	0.22	0.447	3.146	53.3 ± 6.9
		0.25–0.33	8	0.30	0.497	2.852	44.7 ± 7.2
		0.36–0.43	8	0.39	0.542	2.609	29.6 ± 2.7
		0.44–0.66	8	0.56	0.612	2.317	23.2 ± 2.9
		0.68–1.85	7	1.11	0.767	1.836	13.1 ± 3.7

*, ** See Table 3.

instead of Ti containers (Urusov et al., 1997, p. 320). However, a principally important condition of the application of the SSADSC technique is using a great number of large enough crystals of reasonably good quality, which makes such replacements unnecessary in this situation.

The insignificant decrease in D^{str} of Au and Pd in the region 49–60 mol % of the jacobsite end member may have a structural reason. Magnetite has an inverted spinel structure (degree of inversion $\lambda = 1$), whereas the structure of jacobsite (Mn ferrite) is similar to normal spinel. Experimental data on unit-cell

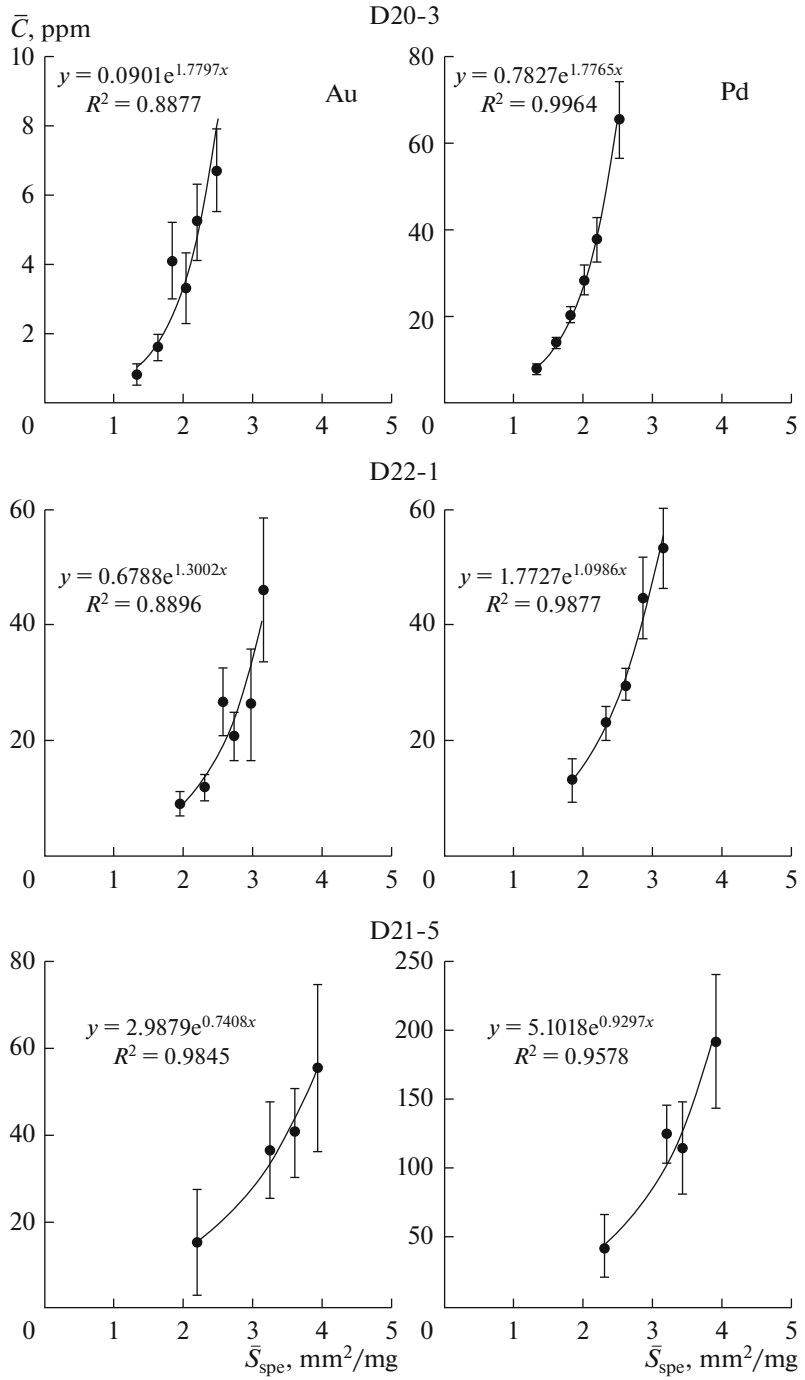

Fig. 2. Dependence of the average concentrations of equally distributed precious metals (Au and Pd) on the specific surface area of an average crystal in size fractions of crystals synthesized at 500°C and containing 0.08 (top row), 18.8 (middle row), and 49.2 (bottom row) mol % of the $MnFe_2O_4$ end member. In the expressions to the left of the curves, the preexponential factor and exponent power correspond to the concentration of the structural admixture of the precious metals and the contribution of the surface-related mode.

parameter–composition dependences are consistent with models in which some Mn^{2+} ions occupy tetrahedral sites and the same or smaller number of Mn^{3+} ions are accommodated at octahedral sites (Taroev and Tauson, 1984). Our data on the parameter–composition dependences for high-Mn samples are mostly consistent with this model at $\lambda = 0.5$. The only exception is sample D18-6, whose data point plots away from the general trend in Fig. 1. It is reasonable to suggest that the structure becomes more or less sharply

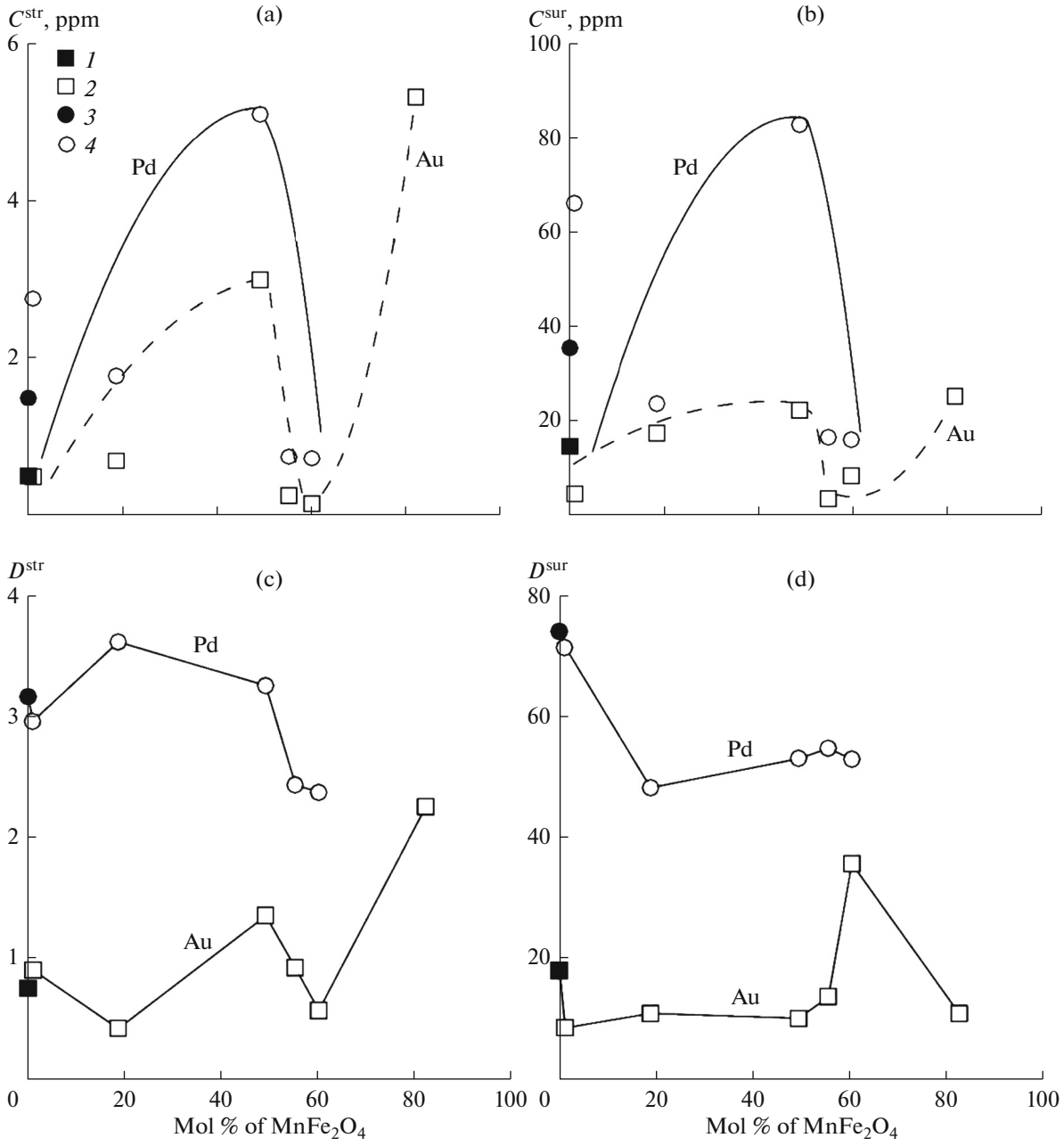

Fig. 3. (a, b) Concentrations of structure- and surface-related modes of Au and Pd occurrence and (c, d) corresponding distribution coefficients of these modes between crystals and fluid depending on the composition of the magnetite–jacobsite solid solution. (*1*, *3*) Au and Pd, respectively, averaged data on "pure" ($\leqslant$0.2 mol % $MnFe_2O_4$) magnetite; (*2*, *4*) Au and Pd, respectively, in the solid solution ($\geqslant$1.3 mol % $MnFe_2O_4$).

less inverted in the region around 50 mol % jacobsite, and this is reflected (although not very clearly) in the distribution coefficients of the Au and Pd structural modes (Fig. 3c).

LA-ICP-MS data. In the context of our research, it is principally important to be able to directly analyze the concentrations of elements on the surface of crystals and in their volumes because the SSADSC technique (Tauson et al., 2013) is not a direct method (regardless of how much it is justified theoretically). The technique has certain serious advantages over other techniques of high spatial resolution, for example, it is less susceptible to the possible heterogeneity of the material and is able to characterize the sample as a whole but not its individual crystals or even a local fragment of a crystal. In the most suitable cases, finite selections (five or six size fractions) comprise no less that 30 individuals, with the rejected crystals also providing information on the modes of occurrence of an admixture (Tauson and Lustenberg, 2008). Such a

Table 5. Concentration (ppm) and distribution coefficients of Au and Pd for the structural and surface-related modes of precious metals in magnetite and manganmagnetite in NH_4Cl[1)] and $NH_4Cl + HCl$[2)] solutions

Experimental run	C_{PM}^{bulk}	C_{PM}^{str}	$\overline{C}_{PM}^{sur}$	D_{PM}^{bulk}	$\overline{D}_{PM}^{bulk}$	D_{PM}^{str}	$\overline{D}_{PM}^{str}$	D_{PM}^{sur}	$\overline{D}_{PM}^{sur}$
Au in Mt*, 450°C									
D13-2[2)]	3.4	0.37	3.33	6.9	26.3	0.78	0.98	6.8	25.2
D18-3[1)]	51.6	1.32	49.11	45.7		1.17		43.5	
Au in Mt-Mn, 450°C									
D13-3[2)]	4.8	0.47	4.30	9.2	11.2	0.90	1.58	8.3	9.4
D18-6[2)]	31.4	5.32	25.05	13.3		2.25		10.6	
Au in Mt, 500°C									
D20-1[1)]	3.1	0.19	2.84	10.7	10.6	0.66	0.52	9.8	10.3
D20-3[1)]	2.4	0.09	2.48	10.4		0.39		10.8	
Au in Mt-Mn, 500°C									
D19-4[2)]	8.1	0.13	8.15	35.2	18.2 ± 13.7	0.57	0.82 ± 0.5	35.4	17.4 ± 9.3
D19-5[1)]	3.6	0.23	3.35	14.4		0.92		13.4	
D21-5[1)]	25.8	2.99	21.98	11.7		1.35		9.9	
D22-1[1)]	18.2	0.68	17.14	11.4		0.42		10.7	
Pd in Mt, 450°C									
D13-2[2)]	27.1	1.18	24.0	60.2	–	2.62	–	53.3	–
Pd in Mt-Mn, 450°C									
D13-3[2)]	60.1	2.75	66.09	64.6	–	2.96	–	71.1	–
Pd in Mt, 500°C									
D20-1[1)]	64.6	2.50	63.68	81.8	86.4	3.16	3.44	80.6	84.0
D20-3[1)]	19.1	0.78	18.34	90.9		3.71		87.3	
Pd in Mt-Mn, 500°C									
D19-4[2)]	15.4	0.71	15.78	51.3	52.0 ± 2.7	2.37	2.92 ± 0.74	52.6	51.9 ± 3.3
D19-5[1)]	15.2	0.73	16.33	50.7		2.43		54.4	
D21-5[1)]	87.0	5.10	82.77	55.4		3.25		52.7	
D22-1[1)]	24.9	1.77	23.47	50.8		3.61		47.9	

* Pure magnetite (*Mt*) is assumed to be a magnetite crystal containing $MnFe_2O_4 \leq 0.2$ mol %. C_{PM}^{bulk} is the bulk concentrations of evenly distributed precious metals in the sample determined from data of Tables 3 and 4 with regard for the average crystal mass and the representativeness of the fraction; C_{PM}^{str} is the PM concentration in the volume (structure) of a crystals found by extrapolating the $\overline{C}_{PM} - \overline{S}_{spe}$ dependence to $S_{spe} = 0$, i.e., to a hypothetic infinite crystal; $\overline{C}_{PM}^{sur}$ is the average concentration of surface-related mode of precious metals calculated by formula (1); Δ is reported for 90% confidence level.

selection practically cannot be representatively characterized by data obtained by analytical techniques of high spatial resolution. However, inasmuch as SSADSC coupled with atomic absorption is not sensitive enough to certain elements (for example, Pt), it is interesting to compare its results with those obtained using direct techniques.

In the course of analysis, the principal mass spectrometer settings were adjusted and optimized according to the proprietary manufacturer manual. The plasma power was 1400 W, the carrier gas (Ar) flow rate was 0.8 L/min, and the rates of the auxiliary flows (Plasma/Cool, Auxiliary Gas) were 20 and 2 L/min. Thanks to the high scanning rate of the quadrupole

Table 6. Proportions of structure- and surface-related modes of Au and Pd occurrence and their distribution coefficients

Element	Number of measurements*	C^{str}/C^{sur}	D^{sur}/D^{str}
Au	10	0.07 ± 0.03	14.3
Pd	9	0.05 ± 0.01	20

* See Table 5; anomalous data on Au in D18-6 are rejected.

Table 7. Structure- and surface-related modes of occurrence depending on the composition of the $FeFe_2O_4$–$MnFe_2O_4$ solid solution

Mol % $MnFe_2O_4$	Au^{str}	Au^{sur}	Pd^{str}	Pd^{sur}
0.1	0.19	2.84	2.50	63.68
0.1	0.09	2.48	0.78	18.34
0.2	0.37	3.33	1.18	24.0
1.3	0.47	4.30	2.75	66.09
18.8	0.68	17.14	1.77	23.47
49.2	2.99	21.98	5.10	82.77
55.3	0.23	3.35	0.73	16.33
60.1	0.13	8.15	0.71	15.78
82.2	5.32	25.05	n.d.	n.d.

mass spectrometer, 63 scans per minute could be recorded, and this allowed us to clearly distinguish variations in the material flux with time. The YAG:Nd laser platform (laser with a 213 nm wavelength) was optimized for aerosol transfer with He along the shortest distance to the mass spectrometer torch, at a He flow rate of 0.6 L/min. The laser power was set at 30%, the laser energy was 0.038 mJ, the frequency of fired pulses was 10 Hz, and the diameter of the laser beam spot was 100 μm. Laser beam passed six times along a straight-line profile on the sample to be analyzed, at a rate of 70 μm/s apart, so that the first and last spots occurred outside the sample, and with the beam focused 1.5 μm deeper in each newly started profile. The crystal and the ablation profile were arranged in such a way that the sample was moved beneath the laser beam by a single engine, and hence, the sample was moved along a single axis to achieve more accurate positioning and an as little as possible varying velocity of the sample. Because the end points of the profiles were outside the sample, we were able to clearly distinguish between the mass spectrometric data of all six ablation passes on the sample and eliminate the effect of deeper laser ablation of the material at the beginning of the profiles because of the extra time needed to accurately position the laser ablation platform. The calibration for the elements to be analyzed was carried out using the NIST 612 standard.

The ablation depth was controlled by a FEI Company Quanta 200 scanning electron microscope at the Electronic Microscopy Center of the Joint Center for Ultramicroanalytical Techniques of the Institute of Limnology, Siberian Branch, Russian Academy of Sciences, in Irkutsk. The measurements were conducted on a number of crystals by determining the focal lengths at natural plain areas at crystal faces and in ablation grooves (Fig. 4). The measured depth range was 6 to 11 μm. In constructing the plots of element distributions with depth (Fig. 5), we assumed an average value of 9 μm. Figure 4 shows the surface of magnetite and the trace of six laser-beam ablation passes on it.

The results obtained on crystals of "pure" and Mn-bearing magnetite are presented in Table 8 and displayed in Fig. 5. The reproducibility of data on individual crystals is relatively low and strongly depends on the state of their surfaces. Nevertheless, these data led us to conclude that the major patterns in the behavior of the analyzed elements with depth are the same. One of the reasons for the variability of the results is the instability of the surface layer of the NP (oxihydroxide; Tauson et al., 2012) under the laser beam. This results in the local swelling and the development of a heterogeneous film on the surface (Fig. 4).

Table 8 shows the analyzed Mn, Au, and Pd concentrations in the first surface layer C^{I}, up to a depth of 1.5 μm, and averaged data on the next five layers (1.5 to 9 μm). These data are given in comparison with the bulk atomic-absorption data on Mn and SSADSC data on Au and Pd concentrations in the structural and surface-related modes. In Fig. 5, LA-ICP-Ms data on discrete layers are shown as rectilinear segments parallel to the abscissa, dashed lines show their averages (without first layer), and dash-dot lines display SSADSC data on the structural modes (for Mn, these are its bulk concentrations as analyzed by atomic absorption). The LA-ICP-MS data testify that the surface of the magnetite is strongly enriched in Mn, as has already been demonstrated by XPS data (Tauson et al., 2013). Our results mostly indicate that surface layer I (and sometimes both layers I and II) are also enriched in Au and Pd. Data on Au (without layer I) are in certain instances in good agreement with SSADSC data on C^{str} (D20-1 and D20-3), and the discrepancies in other cases amount to one order of magnitude, which seems to also be a reasonably good consistency with regard for the principally different nature of these techniques. The discrepancies between C^{I} and C^{sur} (Table 8) are more significant, with C^{I} being always lower. This is understandable because the NP layer concentrating Au and Pd is much thinner, 300 nm or less (Tauson et al., 2012), and data on the 1.5-μm layer are thus significantly "diluted" by volume material. The values converge if the proportions of masses of the element and matrix material in the layers are taken into account.

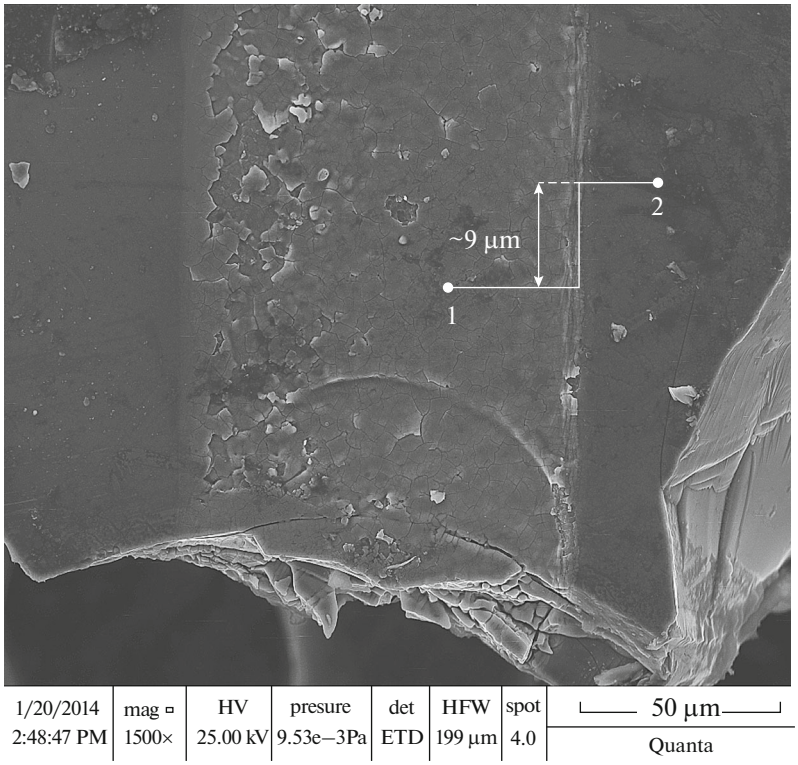

Fig. 4. Focal length measured at plain surface areas (spot 2) and in the zone of the laser beam trajectory (spot 1).

DISCUSSION

The distribution of precious metals in mineral–fluid systems still attracts inadequately little attention of experimentalists, as evident, for example, when publications on this problem are compared with numerous studies devoted to distribution of precious metals between sulfide and silicate liquids, minerals, and silicate melts (Brenan et al., 2003; Capobianco et al., 1994; Fleet et al., 1999). As was mentioned above, fluids are believed to play an important role in the origin of PGE deposits of various types (Li and Ripley, 2005). This seems to pertain even more to Au deposits, which are often of hydrothermal genesis (Kravtsova, 2010). The parameters and mechanisms of processes concentrating ore metals and the role of certain minerals in these processes, speciation of ore elements, and the compositions of ore-forming fluids cannot be understood without comprehending the laws that govern the distribution of precious metals in these heterogeneous systems. This is particularly important in the context of recently obtained data on the distribution of Au and some other elements (Tauson et al., 2011; 2012, 2013; 2014) that shed light onto a new mechanism concentrating elements in naturally occurring mineral crystals in the course of endogenic ore-forming processes. Dependences of the concentrations of minor elements on the crystal size of minerals are now reliably established for experimental and naturally occurring systems (Tauson et al., 2009; 2010,

Table 8. Concentrations (ppm) of elements in the first surface layer ($C^{I} \leqslant 1.5$ μm) and averaged data on the next five layers ($\bar{C}^{II\text{-}VI}$ from 1.5–3 to 7.5–9 μm): LA-ICP-MS data in comparison with atomic-absorption (Mn) and SSADSC (Au and Pd) data

Experimental run	Mn			Au				Pd			
	C^{I}	$\bar{C}^{II-VI}$	C_{AA}	C^{I}	$\bar{C}^{II-VI}$	C^{sur}	C^{str}	C^{I}	$\bar{C}^{II-VI}$	C^{sur}	C^{str}
D20-1	790	64	200	0.6	0.07	2.8	0.19	0.8	0.45	63.7	2.50
D20-3	1470	70	200	0.3	0.19	2.5	0.09	0.4	0.18	18.3	0.78
D22-1	69680	33060	44600	0.06	0.03	17.1	0.68	3.3	1.79	23.5	1.77
D19-4	241450	93150	142900	0.2	0.02	8.1	0.13	0.3	0.11	15.8	0.71

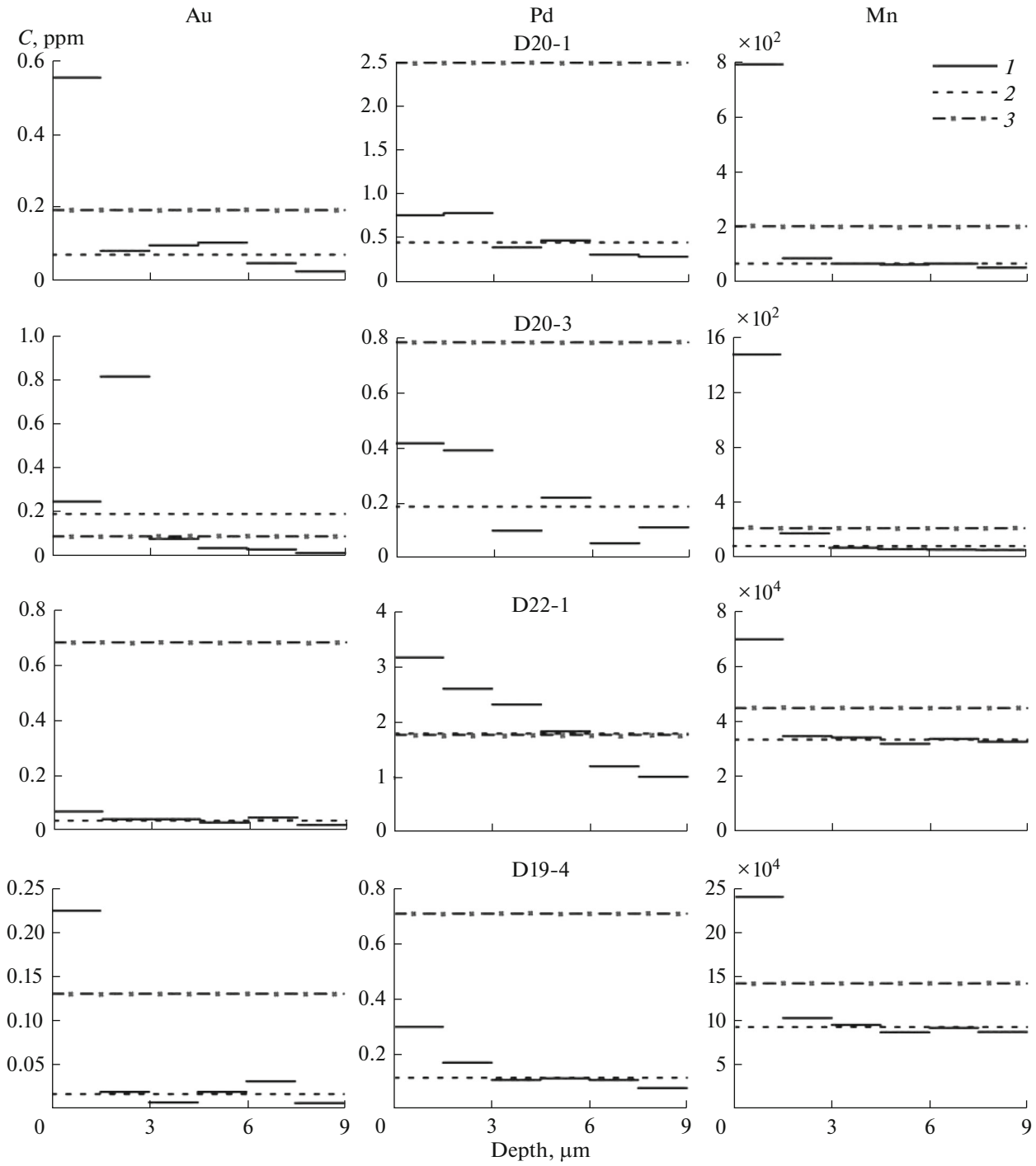

Fig. 5. LA-ICP-MS data on Mn, Au, and Pd distribution with depth in crystals of magnetite (D20-1 and D20-3) and manganmagnetite (D22-1 and D19-4). (*1*) Average concentrations of the elements in the surface layer 1.5 μm thick and next layers (1.5–3 μm and below); (*2*) average concentrations of the elements in the layers form 1.5 to 9 μm; (*3*) concentrations of the structural modes of the elements: SSADSC data on Au and Pd and AAS data on Mn.

2014). The nature of these dependences was first not understood because "normal" adsorption cannot any significantly increase the concentration of elements at elevated temperatures and pressures (Tauson et al., 2005). It is well known that adsorption is an exothermal process and should weaken with increasing temperature according to the Le Chatelier's rule. Because of this, the dependence of the concentrations of minor and trace elements on the size of crystals is thought not to be anyhow related to surface enrichment of

minerals but is explained by differences between generations of the mineral that were formed during certain episodes in the evolutionary history of the deposit. Such interpretations are frequent in the literature (Large et al., 2009). However, newly obtained experimental data and spectroscopic and microscopic studies of the surfaces of minerals demonstrate that these interpretations are not realistic. These data led us to conclude that the dependence of the concentrations of minor and trace elements on the crystal size of minerals can be explained by the occurrence of nanometer-sized nonautonomous phases on the surface of sulfide and oxide minerals growing from hydrothermal solutions. The nonautonomous phases are produced by the chemical modification and structural reconstruction of the surfaces of the crystals during their interaction with the mineral-forming medium (Tauson et al., 2010). For magnetite, the most probable composition of this phase was determined by XPS as oxihydroxide, similar to goethite but with a mixed valence of Fe and vacancies on cation sites (Tauson et al., 2012). The formula that was presented in the aforementioned publication and was slightly modified afterwards is $Fe^{3+}_{1+x}Fe^{2+}_{1-x}\left[O^{2-}_{1+y}(OH)^{-}_{1-y}\right]V^{-}_{2-y+x}$, where V^{-} denotes cation vacancies. This formula can be compared with that of hydromagnetite, which was obtained by oxidizing hydrolysis of Fe(II) salts $Fe^{3+}_{1.8}Fe^{2+}_{0.9}\left[O^{2-}_{3.2}(OH)^{-}_{0.8}\right]V^{-}_{0.3}$ (Kovalenko et al., 2001). LA-ICP-MS data (Fig. 5) indicate that this surface phase is able to significantly concentrate Mn, which can be contained in both bi- and trivalent state and substitute the corresponding cation Fe (Tauson et al., 2013). We believe that this phase is also responsible for the uptake of elevated amounts of precious metals and thus for the dualistic nature of the distribution coefficients of these metals between minerals and fluid. Cations of these metals can interact with the hydroxyl ion and with surface cation vacancies.

Among light PGE, Pd is reportedly the weak incompatible element with magnetite and hematite ($D = 0.7 \pm 0.3$) during the crystallization of silicate melts, in contrast to Ru and Rh ($D \approx 100$–4000 and 250 ± 120, respectively) (Capobianco et al., 1994). The authors of this publication mention the differences in the compatibility of Rh, Rh, and Pd and believe that a spinel phase may play a significant role in defining PGE fractionation trends in, for example, rocks crystallizing at high oxygen fugacity at which PGE occur in oxidized modes. It is uncertain as to how this situation should change in the course of postmagmatic processes under the effect of highly mineralized chloride solutions, which can be of either magmatic or younger hydrothermal origin. Our data obtained in this and earlier studies (Tauson et al., 2012) show that both Pd and Au behave in these environments as elements compatible with magnetite and its solid solutions ($D \sim 3$ and 1, respectively), although Au displays a weak tendency toward preferable enrichment in fluid compared to magnetite ($D \sim 0.5$–0.8) at 500°C. The trends of postmagmatic Pd and Au fractionation can thus significantly depend on the presence of spinel minerals, first and foremost, magnetite and its solid solutions. Concentrations of the structural modes of Pd and Au in these minerals determined by SSADSC and LA-ICP-MS methods may serve as criteria of the operation of overprinted hydrothermal processes. It is also important to stress that the dualistic nature of the distribution coefficients provides reasons to believe that both elements turn out to be highly compatible if not only their structural but also surface-related modes are taken into account ($D^{sur} \approx 17$ and ≈ 50–70 for Au and Pd, respectively).

Magnetite is traditionally thought to become a concentrator of Au and other precious metals in the absence of sulfides, but it is so far uncertain whether this is explained by the crystal chemistry of this mineral or by some other factors. Spinel structures (magnetite, magnesioferrite, chromite, etc.) are thought to be crystal-chemically convenient matrices for accommodation of PGE, and these minerals may be responsible for the concentration of these elements under oxidizing conditions and at significant depths, at which sulfides are thermodynamically instable (Righter and Downs, 2001). Judging from data in (Smagunov and Tauson, 2003), relatively much Au can be accommodated in magnetite, which is practically never saturated with this element. Studying Au distribution in the pyrite–pyrrhotite–magnetite ternary system has shown that magnetite can concentrate roughly as much Au as pyrrhotite does, and the bulk and structural D values of these minerals are similar (Tauson et al., 2013). Because of this, both minerals can closely similarly control Au behavior in hydrothermal systems (in the absence of other effective concentrators, such as pyrite). Magnetite produced by the oxidation of primary pyrrhotite (see the Introduction section above) can be enriched in Pd because of the relatively high D^{str} and D^{sur} values of this element but not because Pd is introduced by younger hydrothermal solutions. The dualistic nature of the distribution coefficients and a significant role of structural defects of crystalline phases and their surface (as the largest defect in crystals, according to Urusov et al., 1997) in the distribution of minor and trace elements demonstrate that a compatible or incompatible behavior of an element with a mineral depend on the modes in which this element is contained in the mineral, and these modes should be elucidated when geochemical and genetic conclusions are derived (Tauson, 1999, 2005).

CONCLUSIONS

Because adsorption is an exothermal process, the adsorption of minor and trace elements according to the mechanism of surface complexation becomes less important at high temperatures, with the accommoda-

tion of elements (first of all, incompatible, although compatible too) in surface nanometer-sized phases becoming more efficient. Minor and trace elements form individual nanophases or are incorporated into similar phases of other elements because this is thermodynamically advantageous over the chemosorption of these elements on the surface of minerals. The physicochemical nature of these phases is still not fully understood, but their ability to accommodate elements that were previously considered incompatible (for example, precious metals) receives more and more supporting arguments, including those presented above. This ability implies the dualistic nature of the distribution coefficients of elements. In chloride hydrothermal solutions at 450 and 500°C, the "surface" distribution coefficient of precious metals between magnetite (manganmagnetite) and hydrothermal solution (D^{sur}, which pertains to precious metals in the surface layer of the crystal) is much higher (by a factor of 14 for Au and 20 for Pd) than the "structural" distribution coefficient (D^{str}).

In the $FeFe_2O_4$–$MnFe_2O_4$ system, the concentrations of structural modes of precious metals increase with increasing concentration of the Mn end member of magnetite from ~0.1 to 49 mol %: the concentration of Au^{str} increases from 0.1 ppm in "pure" magnetite to 3 ppm in Mn-bearing magnetite, and the concentration of Pd^{str} simultaneously increases from 0.8 to 5.1 ppm. An increase in the Mn concentration of magnetite is associated with a decrease in the percentage of precious metals contained in surface-related modes because the surface gradually gets rid of nonautonomous phases. At higher concentrations of the Mn end member (55–60 mol %), the concentrations of both structural and surface-related modes of Au and Pd occurrence decrease to values typical of "pure" magnetite, which may be explained by a decrease in the degree of the structure inversion at approximately 50 mol % jacobsite.

The Mn and Fe cocrystallization coefficient in magnetite is approximately 0.01 within a broad range of the Mn/Fe ratio and weakly depends on temperature within the range of 450–500°C, which makes it possible to use this coefficient to estimate this ratio in the ancient fluid from the composition of magnetite.

During the postmagmatic episode, Pd and Au behave as compatible elements (their D^{str} are approximately 3 and 1, respectively) in the presence of highly mineralized chloride solutions, although Au shows a weak tendency toward preferable enrichment in the fluid as compared to magnetite ($D^{str} \sim 0.5$–0.8) at 500°C. The trends of magmatic Pd and Au fractionation may significantly depend on the presence of spinel minerals, first of all, magnetite and its solid solutions. The Pd and Au concentrations in structural modes depend on the intensity of overprinted hydrothermal processes, and the dualistic nature of the distribution coefficients provides grounds to believe that both elements are then highly compatible with magnetite, if not only structural but also surface-related modes of occurrence of these elements ($D^{sur} \approx 17$ and ≈50–70 for Au and Pd, respectively) are taken into account.

Applied together with electron scanning probe microscopy, LA-ICP-MS can be successfully utilized to obtain data on the concentrations of structural and surface-related modes of occurrence of minor and trace elements. Manganese was proved to be uptaken in the surface layers of magnetite crystals and is likely accommodated in a nonautonomous phase (NP) of oxi-hydroxide (like goethite) composition, which contain Fe in various valence states and Mn(II) and Mn(III) that substitute Fe. The uptake of elevated Au and Pd concentrations by such phases is explained by the interaction of corresponding cations with the hydroxyl anion and cation vacancies in the structure of this NP. Because LA-ICP-MS is a local technique and because NP is unstable under a laser beam, results obtained by this technique are not as stable as SSADSC one but can still be very useful when polymineralic associations and anhedral mineral individuals are studied and when it is difficult to obtain SSADSC data.

ACKNOWLEDGMENTS

The authors thank T.S. Krasnoshchekova, T.M. Voronova, E.V. Savenkova, and L.P. Feoktistova for assistance with analytical studies. This study was financially supported by the Russian Foundation for Basic Research (project no. 12-05-00144 and 13-05-00308) and the Division of Earth Sciences of the Russian Academy of Sciences (Integration Project ONZ-5.1).

REFERENCES

V. V. Akimov and V. L. Tauson, "Accumulation of trace elements in mosaic and micrograined mineral crystals: experimental data," Geochem. Int. **41** (11), 1201–1210 (2003).

B. L. Belykh, N. I. Skripov, V. V. Akimov, V. L. Tauson, T. P. Stepanova, and F. K. Shmidt, "The state of palladium in the nano-sized hydrogenation catalysts modified with elemental phosphorus," Russ. J. General Chem. **83** (12), 2260–2271 (2013).

A. E. Boudreau and W. P. Meurer, "Chromatographic separation of the platinum-group elements, gold, base metals and sulfur during degassing of a compacting and solidifying igneous crystal pile," Contrib. Mineral. Petrol. **134**(2–3), 174–185 (1999).

J. M. Brenan, C. F. Finnigan, W. F. McDonough, and V. Homolova, "Experimental constraints on the partitioning of Ru, Ir, Pt and Pd between chromite and silicate melt: the importance of ferric iron," Chem. Geol. **302–303**, 16–32 (2012).

J. M. Brenan, W. F. McDonough, and C. Dalpe, "Experimental constraints on the partitioning of rhenium and some platinum-group elements between olivine and sil-

icate melt," Earth. Planet. Sci. Lett. **212** (1–2), 135–150 (2003).

C. J. Capobianco, R. L. Hervig, and M. J. Drake, "Experiments on crystal/liquid partitioning of Ru, Rh and Pd for magnetite and hematite solid solutions crystallized from silicate melt," Chem. Geol. **113** (1–2), 23-43 (1994).

L. L. Chyi and J. H. Crocket, "Partition of platinum, palladium, iridium, and gold among coexisting minerals from the deep ore zone, Strathcona Mine, Sudbury, Ontario," Econ. Geol. **71** (7), 1196–1205 (1976).

J. E. Collins, S. J. Barnes, S. G. Hagemann, T. C. McCuaig, and K. M. Frost "Postmagmatic variability in ore composition and mineralogy in the T4 and T5 ore shoots at the high-grade Flying Fox Ni–Cu–PGE deposit, Yilgarn Craton, Western Australia," Econ. Geol. **107** (5), 859–879 (2012).

J. H. Crocket, Y. Teruta, and J. Garth, "The relative importance of sulfides, spinels, and platinoid minerals as carriers of Pt, Pd, Ir, and Au in the Merensky Reef at Western Platinum Limited, near Marikana, South Africa," *Econ. Geol.* **71** (7), 1308–1323 (1976).

S. A. S. Dare, S.-J. Barnes, and G. Beaudoin, "Evolution of trace element concentrations in magnetite from a fractionating magmatic sulfide liquid: an example from the Sudbury (Canada) Ni–Cu–PGE deposits," in *11th SGA Biennial Meeting.* (Univ. Catal. Norte, Antofagasta, 2011), pp. 621–623.

M. Economou-Eliopoulos and D. G. Eliopoulos, "Mineralogical and geochemical characteristics of the Skouries porphyry–Cu–Au–Pd–Pt deposit (Greece): evidence for the precious metal," in *Mineral Deposit Research: Meeting the Global Challenge,* Ed. by J. Mao and F. P. Bierlein (Springer, Berlin–Heidelberg, 2005), pp. 935–938.

M. E. Fleet, J. H. Crocket, M. Liu, and W. E. Stone "Laboratory partitioning of platinum-group elements (PGE) and gold with application to magmatic sulfide-PGE deposits," Lithos **47** (1–2), 127–142 (1999).

Yu. A. Kovalenko, A. M. Nugmanov, and L. Yu. Firsova, "The influence of synthesis conditions on magnetite structure imperfection," Russ. J. Phys. Chem. A **75** (11), 1983–1087 (2001).

R. G. Kravtsova, *Geochemistry and Conditions of the Formation of Gold–Silver Ore-Forming Systems of the Northern Okhotsk Region* (Geo, Novosibirsk, 2010) [in Russian].

R. R. Large, L. Danyushevsky, C. Hollit, V. Maslennikov, S. Meffre, S. Gilbert, S. Bull, R. Scott, P. Emsbo, H. Thomas, B. Singh, and J. Foster, "Gold and trace element zonation in pyrite using a laser imaging technique: Implications for the timing of gold in orogenic and Carlin-style sediment-hosted deposits," Econ. Geol. **104** (5), 635-668 (2009).

C. Li and E. M. Ripley, "The roles of fluid in the genesis and modification of reef-type PGE deposits in large layered intrusions," Geochim. Cosmochim. Acta **69** (10), A332 (2005).

V. I. Men'shikov, I. Yu. Voronova, O. A. Proidakova, S. F. Malysheva, N. I. Belogorlova, N. K. Gusarova, and B. A. Trofimov, "Preconcentration of gold, silver, palladium, platinum, and ruthenium with organophosphorus extractants," Russ. J. Appl. Chem. **82** (2), 183–189 (2009).

A. J. Naldrett, J. Singh, S. Krstic, and C. Li, "The mineralogy of the Voisey's Bay Ni–Cu–Co deposit, Northern Labrador, Canada: influence of oxidation state on textures and mineral compositions. Econ. Geol. **95** (4), 889-900 (2000).

R. Piña, F. Gervilla, S.-J. Barnes, L. Ortega, and R. Lunar, "Platinum-group elements-bearing pyrite from the Aguablanca Ni-Cu sulphide deposit (SW Spain): a LA–ICP–MS study," Eur. J. Mineral. **25** (2), 241–252 (2013).

T. D. Radhakrishnan Nair, and C. U. Aniz, "Effect of redox nature of impregnated ferrite catalysts on their carbon monoxide oxidation activity," *Res. Rev.: J. Mater. Sci.* **1** (2), 45–52 (2013).

K. Righter and R. T. Downs, "The crystal structures of synthetic Re- and PGE-bearing magnesioferrite spinels: Implications for impacts, accretion and the mantle," *Geophys. Res. Lett.* **28** (4), 619–622 (2001).

N. V. Smagunov and V. L. Tauson, "Magnetite and pyrrhotite as potential gold concentrators at low sulfur activity," Dokl. Earth Sci. **392** (7), 995–998 (2003).

V. L. Tauson and V. V. Akimov, "Introduction to the theory of forced equilibria: General principles, basic concepts, and definitions," Geochim. Cosmochim. Acta **61** (23), 4935–4943 (1997).

V. K. Taroev and V. L. Tauson, *Analysis of "Unit Cell Parameters–Composition" Correlations in Spinel Systems with Magnetite* (IGKh SO RAN, Irkutsk, 1984) [in Russian].

V. L. Tauson, "Endocrypty: modern concepts and investigation techniques," Geochem. Int. **37** (6), 588–591 (1999).

V. L. Tauson, "Systematics of processes of trace element uptake by real mineral crystals," Geochem. Int. **43** (2), 184–190 (2005).

V. L. Tauson, "The Principle of Continuity of Phase Formation at Mineral Surfaces," Dokl. Earth Sci. **425A** (3), 471–475 (2009).

V. L. Tauson and S. V. Lipko, "Pyrite as a concentrator of gold in laboratory and natural systems: a surface-related effect," in *Pyrite: Synthesis, Characterization and Uses. Chapter 1* Ed. by N. Whitley and P. T. Vinsen (Nova Sci. Pub. Inc., New York, 2013), pp. 1–40.

V. L. Tauson and E. E. Lustenberg, "Quantitative determination of modes of gold occurrence in minerals by the statistical analysis of analytical data samplings," Geochem. Int. **46** (4), 423–427 (2008).

V. L. Tauson, I. Yu. Parkhomenko, D. N. Babkin, V. I. Men'shikov, and E. E. Lustenberg, "Cadmium and mercury uptake by galena crystals under hydrothermal growth: a spectroscopic and element thermorelease atomic absorption study," Eur. J. Mineral. **17** (4), 599–610 (2005).

V. L. Tauson, T. M. Pastushkova, D. N. Babkin, T. S. Krasnoshchekova, and E. E. Lustenberg, "Effect of particle size variation in a sample on trace element concentration," Dokl. Earth Sci. **429** (6), 1590–1596 (2009).

V. L. Tauson, T. M. Pastushkova, D. N. Babkin, T. S. Krasnoshchekova, and E. E. Lustenberg, "The effect of the crystal size in sample on the trace-element concentration," Russ. Geol. Geophys. **51** (7), 764–773 (2010).

V. L. Tauson, D. N. Babkin, T. M. Pastushkova, T. S. Krasnoshchekova, E. E. Lustenberg, and O. Yu. Belozerova, "Dualistic distribution coefficients of elements in the system mineral–hydrothermal solution. I. Gold accumulation in pyrite," Geochem. Int. **49** (6), 568–577 (2011).

V. L. Tauson, D. N. Babkin, T. M. Pastushkova, V. V. Akimov, T. S. Krasnoshchekova, S. V. Lipko, and O. Yu. Belozerova, "Dualistic distribution coefficients of elements in the system mineral–hydrothermal solution. II. Gold in magnetite," Geochem. Int. **50** (3), 227–245 (2012).

V. L. Tauson, D. N. Babkin, V. V. Akimov, S. V. Lipko, N. V. Smagunov, and I. Yu. Parkhomenko, "Trace elements as indicators of the physicochemical conditions of mineral formation in hydrothermal sulfide systems," Russ. Geol. Geophys. **54** (5), 687–706 (2013).

V. L. Tauson, R. G. Kravtsova, N. V. Smagunov, A. M. Spiridonov, V. I. Grebenshchikova, and A. E. Budyak, "Structurally and superficially bound gold in pyrite from deposits of different genetic types," Russ. Geol. Geophys. **55** (2), 350–369 (2014).

V. L. Tauson, S. V. Lipko, K. Yu. Arsentev, and N. V. Smagunov, "Formation of multiphase mineral associations and selection of components by growing crystals: interdependent problems of crystal genesis studied by A.E.Glikin and related to superficial nanostructures," in *Abstr. III Internat. Conf. "Crystallogenesis and Mineralogy"* (Publishing House of SB RAS, Novosibirsk, 2013), pp. 204–205.

V. S. Urusov, V. L. Tauson, and V. V. Akimov, *Geochemistry of Solids* (GEOS, Moscow, 1997) [in Russian].

N. Vatin-Perignon, J. Amosse, L. Radelli, F. Keller, and T. Castro Leyva, "Platinum group element behavior and thermochemical constraints in the ultrabasic–basic complex of the Vizcaino Peninsula, Baja California Sur, Mexico," Lithos **53** (1), 59–80 (2000).

Y. Xiong and S. A. Wood, "Experimental quantification of hydrothermal solubility of platinum-group elements with special reference to porphyry copper environments," Mineral. Petrol. **68** (1–3), 1–28 (2000).

Z. Zajacz, J. J. Hanley, C. A. Heinrich, W. E. Halter, and M. Guillong, "Diffusive reequilibration of quartz-hosted silicate melt and fluid inclusions: Are all metal concentrations unmodified?," Geochim. Cosmochim. Acta **73** (10), 3013–3027 (2009).

Translated by E. Kurdyukov